POLİTEKNİK DERGİSİ

JOURNAL of POLYTECHNIC

ISSN: 1302-0900 (PRINT), ISSN: 2147-9429 (ONLINE)
URL: http://dergipark.org.tr/politeknik

Optimization of low-altitude UAV wing design using comparative statistical analysis method

Karşılaştırmalı istatistiksel analiz yöntemi kullanılarak alçak irtifa IHA kanat tasarımının optimizasyonu

Yazar(lar) (Author(s)): Osman ÖZDAMAR[1*], Burak ÖZTÜRK[2], Emre CAN[3], Cengizhan ABAY[4] Tufan İNAÇ[5]

ORCID[1]: 0000-0001-6353-6812

ORCID[2]: 0000-0002-1018-6545

ORCID[3]: 0009-0009-9369-8404

ORCID[4]: 0000-0002-7484-2687

ORCID[5]: 0000-0001-8304-3441

To cite to this article: Özdamar O., Öztürk B., Can E., Abay C. and İnaç T., "Optimization of Low-Altitude UAV Wing Design Using Comparative Statistical Analysis Method", ***Journal of Polytechnic***, 29(2):290213:1-13 (2026).

Bu makaleye şu şekilde atıfta bulunabilirsiniz: Özdamar O., Öztürk B., Can E., Abay C., İnaç T., "Optimization of Low-Altitude UAV Wing Design Using Comparative Statistical Analysis Method", **Politeknik Dergisi**, 29(2):290213:1-13 (2026).

Erişim linki (To link to this article): http://dergipark.org.tr/politeknik/archive

DOI: 10.2339/politeknik.1646366

Optimization of Low-Altitude UAV Wing Design Using Comparative Statistical Analysis Method

Highlights

- *Comparative statistical analysis methods (Taguchi, ANOVA, RSM) were integrated effectively.*
- *An optimized wing geometry was developed specifically for low-altitude UAVs.*
- *Aerodynamic efficiency parameters were evaluated using CFD and FEM analyses.*
- *A maximum lift force of 253 N and a minimum drag force of 10.2 N were achieved.*
- *A custom wireless speed measurement system was developed for real flight tests.*
- *The 6S battery provided a 12.96% increase in flight speed compared to the 5S battery.*

Graphical Abstract

In this study, the optimal wing geometry for low-altitude UAVs was determined using multi-parametric statistical analysis methods.

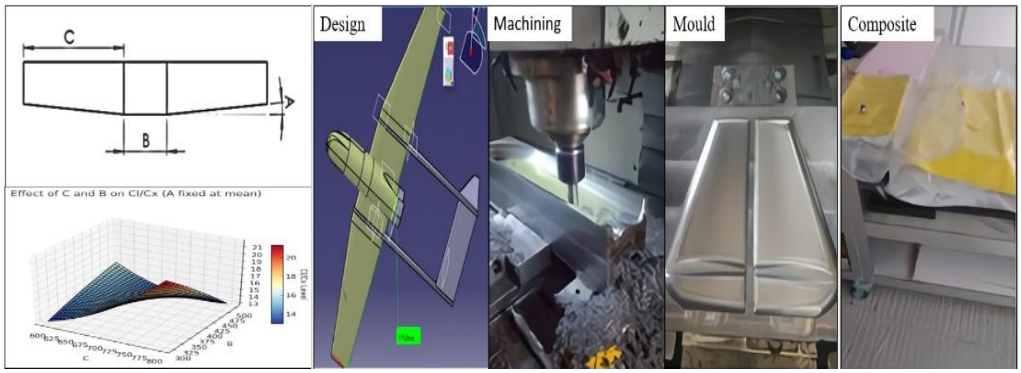

Figure. Stages of the UAV wing optimization process

Aim

This study aims to determine the optimal wing geometry for unmanned aerial vehicles (UAVs) operating at low altitudes. Statistical methods such as RSM, Taguchi, and ANOVA were used to analyze the effects of different parameter combinations on flight performance. Based on the findings, an ideal design that provides maximum lift and minimum drag was developed.

Design & Methodology

Three main parameters were defined and examined at three levels: side wing angle, central wing length, and leading-edge wing length. Data obtained from CFD analyses in ANSYS Fluent were evaluated using ANOVA, Taguchi, and RSM methods in Minitab software. Additionally, a custom wireless speed measurement system was developed, and flight tests were conducted.

Originality

This study goes beyond conventional approaches focused on biomimetic or single-variable analyses in UAV wing design by providing optimization through multi-parametric statistical methods. Moreover, the designed wing geometry was validated through actual flight tests, offering unique contributions for industrial applications.

Findings

The optimal design was achieved with an 8° side wing angle, 400 mm central wing length, and 700 mm leading-edge wing length. This configuration yielded a lift force of 253 N and a drag force of 10.2 N, achieving a CL/CD ratio of 17.6. Furthermore, it was observed that the 6S battery delivered 12.96% higher speeds.

Conclusion

This study identified the optimal wing design for low-altitude UAVs using multi-parametric statistical analysis methods. The designed system offers high performance in terms of both lift force and aerodynamic efficiency. Additionally, the developed speed measurement system validated the theoretical findings through practical testing.

Declaration of Ethical Standards

The author(s) of this article declare that the materials and methods used in this study do not require ethical committee permission and/or legal-special permission.

Optimization of Low-Altitude UAV Wing Design Using Comparative Statistical Analysis

Araştırma Makalesi / Research Article

Osman ÖZDAMAR[1*], Burak ÖZTÜRK[2], Emre CAN[2], Cengizhan ABAY[3], Tufan İNAÇ[4]

[1]Bilecik Şeyh Edebali University, Osmaneli Vocational School of Higher Education, Bilecik.
[2]Bilecik University, Metallurgical and Materials Engineering, Bilecik.
[3]Bilecik Şeyh Edebali University, BAP, Bilecik.
[4]Bilecik Şeyh Edebali University, Electrical Electronics Engineering, Bilecik

(Geliş/Received : 25.02.2025 ; Kabul/Accepted : 30.06.2025 ; Erken Görünüm/Early View : 25.07.2025)

ABSTRACT

Today, unmanned aerial vehicles (UAV) are widely used across various fields, including civil, military, and social activities. Fixed-wing UAV operating at low altitudes typically have a wingspan ranging from 2 to 4 meters and can sustain flight for up to three hours. Their wing structure generally consists of three main components: a central wing that bears the primary structural load, and left and right side wings that are critical for determining flight endurance and speed. The lengths of these components vary, with the side wings designed at an angle to reduce wind resistance and enhance flight speed. In this study, three main parameter levels were identified for an average low-altitude drone, and the optimal dimensions were evaluated using RSM (Response Surface Methodology), the Taguchi method, FEM (Finite Element Method), and Analysis of Variance (ANOVA) analyses. The optimal design was achieved with a central wing length of 400 mm, side wing lengths of 700 mm, and a side wing angle of approximately 8°. Analysis results showed a maximum lift force (F_Z) of 253 N, a minimum drag force of 10.2 N, a maximum lift coefficient (C_L) of 0.66, and a lift-to-drag (C_L/C_D) ratio of 17.6. Based on these findings, composite molds were manufactured for the aircraft, and a testing device was developed to measure speed during flight trials. Under 10 m/s wind conditions, the maximum speed recorded for this optimized geometry was 183 km/h.

Key Word: Wing Design, Low-Altitude UAV, Unmanned Aerial Vehicle Optimization FEM, Aerodynamics.

Karşılaştırmalı İstatistiksel Analiz Yöntemi Kullanılarak Alçak İrtifa İHA Kanat Tasarımının Optimizasyonu

ÖZ

Günümüzde insansız hava araçları (İHA) sivil, askeri ve sosyal faaliyetler de dahil olmak üzere çeşitli alanlarda yaygın olarak kullanılmaktadır. Alçak irtifalarda çalışan sabit kanatlı İHA'lar tipik olarak 2 ila 4 metre arasında değişen kanat açıklığına sahiptir ve üç saate kadar uçuşlarını sürdürebilirler. Kanat yapıları genellikle üç ana bileşenden oluşur: birincil yapısal yükü taşıyan merkezi bir kanat ve uçuş dayanıklılığını ve hızını belirlemek için kritik olan sol ve sağ yan kanatlar. Bu bileşenlerin uzunlukları değişmekte olup, yan kanatlar rüzgâr direncini azaltmak ve uçuş hızını artırmak için açılı olarak tasarlanmıştır. Bu çalışmada, ortalama bir alçak irtifa drone'u için üç ana parametre seviyesi belirlenmiş ve optimum boyutlar RSM (Yanıt Yüzeyi Metodolojisi), Taguchi yöntemi, FEM (Sonlu Elemanlar Yöntemi) ve Varyans Analizi (ANOVA) analizleri kullanılarak değerlendirilmiştir. Optimum tasarım 400 mm merkezi kanat uzunluğu, 700 mm yan kanat uzunluğu ve yaklaşık 8° yan kanat açısı ile elde edilmiştir. Analiz sonuçları 253 N maksimum kaldırma kuvveti (F_Z), 10.2 N minimum sürükleme kuvveti, 0.66 maksimum kaldırma katsayısı (C_L) ve 17.6 kaldırma-sürükleme (C_L/C_D) oranı göstermiştir. Bu bulgulara dayanarak, hava aracı için kompozit kalıplar üretildi ve uçuş denemeleri sırasında hızı ölçmek için bir test cihazı geliştirildi. 10 m/s rüzgar koşulları altında, bu optimize edilmiş geometri için kaydedilen maksimum hız 183 km/s olmuştur.

Anahtar Kelime: Kanat Tasarımı, Alçak İrtifa İHA, İnsansız Hava Aracı Optimizasyonu FEM, Aerodinamik.

1. INTRODUCTION

UAV (Unmanned Aerial Vehicles) are autonomous systems that do not require an onboard pilot and are operated remotely. These vehicles can navigate independently along predefined routes and have recently begun to be integrated with artificial intelligence techno logies [1, 2]. Thanks to significant advancements in radio technology and increased accessibility, UAVs are now widely used across a broad range of industries [3, 4]. Thanks to their unique flight capabilities, state-of-the-art aerial vehicles are now employed in mapping, search-and-rescue operations, weather monitoring, fire surveillance, and agricultural applications, and have recently begun to be used for last-mile deliveries, making these processes more efficient and effective than ever before [5, 6]. UAV technology continues to advance, providing solutions across many aspects of daily life. Ongoing research is focused on optimizing and enhancing their software, propulsion systems, and

* *Sorumlu Yazar (Corresponding Author)*
e-posta : osman.ozdamar@bilecik.edu.tr

structural designs [7]. One of the most important aerodynamic components determining a UAV's flight performance is the wing [8, 9]. Wing design directly impacts a wide range of aerodynamic factors, from lift production to drag resistance [10, 11].

Therefore, especially for low-altitude operations, wing geometry must be meticulously designed to achieve optimal performance. In this context, numerous studies have examined the influence of parameters such as airfoil shape, angle of attack, camber ratio, and wingspan on aerodynamic performance.

In the development of UAV, numerous studies have sought to identify optimal design characteristics for wings and fuselage structures. For example, one investigation focused on reducing aerodynamic noise while enhancing the C_L/L_D ratio of wing profiles. Insights from nature show that owls achieve remarkably quiet flight at low frequencies (2–20 kHz) and owe their superior aerodynamic performance to the specialized morphology of their wings [12]. Another study aimed to reduce UAV propeller noise by drawing inspiration from the leading-edge serrations of owl wings. Five different serrated propeller designs were developed and tested, and the most successful design (a saw-tooth model) achieved an average noise reduction of 2.43 dB along with a 3.53 % increase in thrust. These results indicate that biomimetic serrations can offer both noise attenuation and performance enhancement for UAV [13]. The NACA (National Advisory Committee for Aeronautics) series of airfoil profiles is widely employed-particularly in educational and research analyses. Their aerodynamic performance at various angles of attack and Reynolds numbers has been investigated using CFD simulations and wind-tunnel experiments[14-16]. Gök et al. (2021) investigated the aerodynamic performance of the NACA 2412 and NACA 4412 airfoil profiles at angles of attack ranging from 0° to 20°. Computational Fluid Dynamics (CFD) simulations were carried out in SolidWorks under a steady free-stream velocity of 43 m/s. [17]. Similarly, Pan et al. redesigned an unmanned underwater vehicle inspired by manta rays. By increasing the vehicle's thickness by 9% and employing a NACA0016-based profile, they achieved a 10% improvement in the lift-to-drag ratio [18]. Upasena et al. (2019) drew inspiration from the wing morphology of the Magnificent Frigatebird to design two NACA 2412-based airfoil models-one biomimetic (Frigate-inspired) and one conventional. They carried out ANSYS® 18.1 simulations across a range of angles of attack and Mach numbers, employing both the Spalart Allmaras and k-epsilon turbulence models. The results showed that the biomimetic wing consistently outperformed the conventional profile at low speeds, confirming the aerodynamic benefits of the Frigate-inspired serrations [19]. Martin (2017) investigated the impact of small winglets inspired by pelican wing tips on flight performance. These features were modeled using 3D scanning techniques and CAD software [20]. Focke and colleagues designed a small-scale aerial vehicle inspired by flying fish and reported a 24.5 % increase in lift coefficient alongside a 1.56 % reduction in drag under near-sea-level flight conditions [21]. Murphy (2008) investigated dragonfly wing–inspired, undulated wing structures and found that these designs delay stall (loss of lift) when the angle of attack exceeds 12°[22].

Risanthia et al. (2024) optimized the wing design of a fixed-wing UAV using the Efficient Global Optimization (EGO) algorithm. Initial design samples were generated via Latin Hypercube Sampling (LHS), and the optimization process combined the Expected Improvement (EI) criterion with a Genetic Algorithm (GA). Aerodynamic performance was evaluated using VSPAERO under constraints of fixed wing area and root chord length. By optimizing the maximum thickness-to-chord ratio, wing half-span, and sweep angle, they achieved a 16.56 % increase in the C_L/C_D ratio. A subsequent sensitivity analysis indicated that wing span exerted the greatest influence on overall aerodynamic performance [23]. Kontogiannis et al. (2013) developed an electric UAV for aerial photography and surveillance with targets of a low stall speed (< 12 m/s), a 60 m takeoff run, and a 6 kg payload capacity. By employing an E420 airfoil and optimizing the design via computational fluid dynamics (CFD) analysis (including the addition of small flaps) they achieved a 7.7 % increase in aerodynamic efficiency. Flight tests validated the prototype's performance, demonstrating that it is low-cost, environmentally friendly, and highly maneuverable [24]. With the advancement of numerical analysis techniques, CFD tools have become widely employed for evaluating UAV wing designs. These simulations enable highly accurate examination of details such as pressure distributions within the airflow, boundary layer development, and flow separation regions. Consequently, CFD data serve as a critical foundation both for validating experimental findings and for assessing novel aerodynamic configurations [25, 26]. However, aerodynamic analyses alone are not sufficient; statistical methods are also needed to evaluate multiple design variables simultaneously. By employing these techniques, the effects of various design parameters on UAV performance can be compared and analyzed in concert, enabling the identification of optimal design combinations [27]. Variance analysis (ANOVA), the Taguchi method, Response Surface Methodology (RSM), and regression modeling techniques are employed in this process [28].

A review of the literature reveals that existing studies predominantly focus on limited aerodynamic factors (such as biological anatomical features and angle of attack) while parametric design approaches remain underexplored. In this project, we will perform a comprehensive investigation of parametric wing geometries using a variety of modeling techniques and evaluate their aerodynamic performance through CFD analyses. Specifically, wing designs tailored for low-altitude unmanned aerial vehicles will be assessed via comparative statistical methods across multiple

performance criteria. By moving beyond the single-parameter evaluations typical in the current literature, this study aims both to introduce a novel academic perspective and to produce optimized, practically applicable wing configurations.

2. BASIC FLIGHT THEORY

To effectively demonstrate the flight characteristics of an aircraft, it is essential to meet fundamental aerodynamic requirements, such as achieving a C_L>0.5C_L>0.5 and avoiding stall below 15° angle of attack [29]. These requirements critically influence design trade-offs and performance metrics. Aerodynamically, lift (generated through wing geometry and airflow dynamics) counteracts the aircraft's weight to maintain altitude, while thrust overcomes both parasitic and induced drag components to ensure forward motion. This balance is governed by the Navier-Stokes equations and validated through wind-tunnel testing [30]. Key aerodynamic factors to be considered in aircraft design include wing profile, surface area, wing angle, and flight speed. Optimizing these factors helps increase lift while minimizing drag, thereby improving aerodynamic efficiency. This is crucial for enhancing flight performance and reducing fuel consumption. In this context, the structure of the wings plays a fundamental role in generating lift [31, 32].

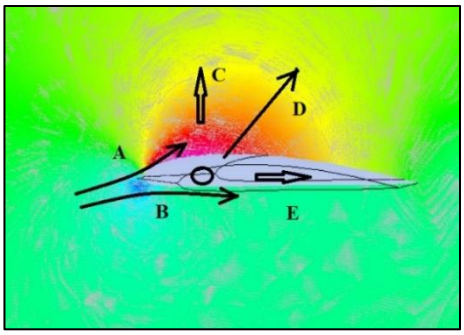

Figure 1. Forces generated during flight.

In Figure 1, the flow pattern and aerodynamic forces around an airfoil in flight are illustrated. The more highly cambered upper surface accelerates the air above the wing (A), while the flow beneath the flatter lower surface moves more slowly (B). According to Bernoulli's principle, an increase in fluid velocity corresponds to a decrease in static pressure; consequently, a low-pressure region forms over the upper surface (C), whereas a relatively higher-pressure region persists beneath the wing. The resulting pressure differential produces an upward net force (depicted by vector D) which is known as lift and constitutes the fundamental aerodynamic effect that keeps aircraft aloft. Vector E indicates the direction of airflow along the lower surface, and the overall diagram highlights the interplay between pressure and velocity distributions around the airfoil [33, 34].

Lift force is one of the fundamental aerodynamic forces that determine the flight performance of an aircraft. This force is influenced by geometrical and flow condition parameters such as angle of attack, blade pitch, aspect ratio, conical ratio and sweep angle. The lift force is generally expressed by the following formula (Equation 1) [29, 36].

$$FL\ (Fd, Fm)\ \frac{1}{2}\ pxAxv^2(CL) \qquad (1)$$

Where: p: Air density (kg/m³), A: Blade surface area (m²), v: Air flow velocity (m/s), C_L: Lift coefficient, F_D: Drag coefficient, FM: Moment coefficient.

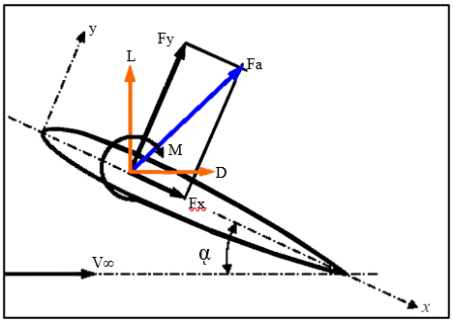

Figure 2. Vector representation of forces [35].

On the other hand, the drag force acts parallel to the free air flow and opposite to the direction of flight. This force is directly related to air speed, wing area, air density and C_D coefficient. The angle of attack, which is one of the parameters most affecting the lift force, is defined as the angle between the wing chord line and the relative wind direction. Increasing the angle of attack generally increases both the lift coefficient (C_L) and drag coefficient (C_D). At low angles of attack, the airflow adheres smoothly to the wing surface, but as the angle increases, this flow begins to separate from the surface and becomes turbulent. The critical angle at which this separation occurs is called the 'stall angle' and is one of the main factors determining the maximum speed and hover time of an aircraft.

The maximum flight time and ideal payload carrying capacity of UAV constitute the basis of the studies for the development of these vehicles. In this direction, researchers have started a project to design a UAV capable of reaching a range of 100 kilometers at a speed of 180 kilometers per hour and carrying a payload of 2 kilograms. In particular, the aerodynamic structure of the wings and general aircraft design features are among the critical elements that directly affect the payload capacity and ensure optimum performance in terms of speed. For this reason, within the scope of the project, firstly, studies were carried out to determine the optimum parameters for the wing design.

3. MATERIALS AND METHODS

This research, developed to create an optimal wing design, was completed in three main stages, as shown in Figure 3. These stages are: design optimization (a), mold and aircraft manufacturing (b), and flight speed testing (c). In the first stage, comparative statistical analyses were conducted during the design process, and the optimal wing geometry was determined based on the

results. In the second stage, molds of the low-altitude UAV with the optimum wing design were manufactured, and mechanical assembly was performed. In the final stage, electronic hardware was assembled, and maximum speed tests were conducted in 10 m/s airflow conditions.

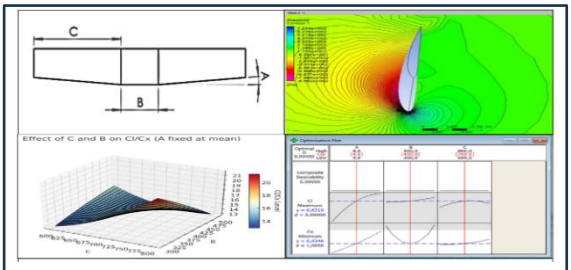

Optimization in Design Based on FEM, RSM Taguchi, and ANOVA Analysis

Mould Manufacturing, Composite Production and Mechanical Assembly of Optimum Design Geometry

Electronic Assembly and Flight Speed Tests

Figure 3. Experiment Organization Chart.

A wing consists of two primary sections: the central wing and side wings. The central wing typically features a flat, non-angled design and plays a critical role in bearing static loads. Side wings, on the other hand, are generally designed with specific angles to enhance flight speed (Figure 4). However, in designs where load-bearing capacity is prioritized and speed is kept minimal, side wings are also produced without angles. In this project, the necessary design criteria were thoroughly examined to achieve both maximum load capacity and ideal speed performance. To this end, advanced statistical methods such as RSM, the Taguchi method, and ANOVA were used for comparative analysis. As a result of these analyses, the optimum parametric design criteria were identified, and a wing geometry meeting these criteria was developed.

This study aims to develop an UAV that can fly with a 20-35 cc internal combustion engine or a brushless engine capable of providing 4-5 kg thrust. In the industry, such UAV usually have a wingspan of 1.8 meters. Accordingly, the minimum and maximum dimensions of the three design parameters were determined (Table 1) and statistical analyses were performed to determine the factors affecting the maximum payload and flight speed.

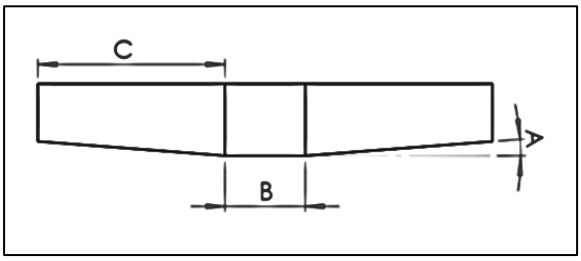

Figure 4. Wing length and angle parameters.

As seen in Figure 4, wing B is positioned as the center wing in the carrier configuration and the main structural connections are established in this section. Wing C serves as the leading-edge wing, while wing A represents the lateral wing angle. The dimensions given in the table represent the standard minimum and maximum dimensions for low-altitude UAV.

Table 1. Experimental Design of Parameters.

Experiment No.	**A** Analiz Kodu	**B** Analiz Kodu	**C** Analiz Kodu	**A**, (Side Wing Angle Deg.)	**B**, (Middle Wing, mm)	**C**, (Leading Edge, mm)
1	1	1	1	8	300	600
2	1	2	2	8	400	700
3	1	3	3	8	500	800
4	2	1	2	4	300	700
5	2	2	3	4	400	800
6	2	3	1	4	500	600
7	3	1	3	0	300	800
8	3	2	1	0	400	600
9	3	3	2	0	500	700

This table 1 is designed to test different levels of three key parameters (side wing angle, center wing size and leading edge length) that affect performance in an UAV wing design. This partial factorial design, consisting of a total of 9 experiments, includes three levels (1, 2, 3) of each parameter and the actual values corresponding to these levels. The side wing angle (A) is defined as 8° in code 1, 4° in code 2 and 0° in code 3. The center wing size (B) is defined as 300 mm (code 1), 400 mm (code 2) and 500 mm (code 3), and the leading edge length (C) as 600 mm (code 1), 700 mm (code 2) and 800 mm (code 3), respectively.

The experiments were organized to cover combinations between minimum (A: 0°, B: 300 mm, C: 600 mm) and maximum (A: 8°, B: 500 mm, C: 800 mm) values of the parameters. For example, in Experiment 1 the side wing angle was 8°, the center wing size was 300 mm and the leading edge length was 600 mm, while in Experiment 7 these values were set to 0°, 300 mm and 800 mm. This design was created to statistically analyses (by ANOVA or regression analysis) the effects of the parameters on performance indicators such as payload, stability and speed.

The side wing angle (A) parameter shows a decrease in angle value as the code level increases, while the centre wing size (B) and leading edge length (C) parameters

show a linear increase with code level. This structure shows that the wing geometry scales systematically and provides a consistent basis for performance optimization. The data obtained will be used to determine critical parameter combinations to improve the aerodynamic efficiency of the UAV.

3.1 System Testing Methodology

ANOVA was developed by Sir Ronald A. Fisher and is used to assess whether the means between different groups are statistically significantly different. The F-statistic obtained in this analysis is based on the ratio of between-group and within-group variances and significance is determined by the p-value corresponding to this ratio. The Taguchi method is an approach to optimizing quality in experimental design; the orthogonal arrays used allow factors to be tested independently of each other and, when used in combination with ANOVA, the decomposition of variance into its components becomes easier and more reliable. Therefore, ANOVA and Taguchi methods together allow systematic and meaningful analyses of experimental data [37, 38]. Optimization was performed using ANOVA and Taguchi methods, while lift (C_L), drag (C_D), vertical force (F_Z), lateral force (F_Y) and C_L/C_D were measured using Finite Element Method (FEM) and Fluent flow analysis. S/N ratios were used to optimize the control factors. The results evaluated safety factors, stress levels and volume to improve product quality, cost efficiency and durability (Equation 2).

$$\text{Nominal is the best } = 10\, log\left(\frac{\bar{y}}{s_{\bar{y}}^2}\right) \qquad (2)$$

In Equation 2, the following symbols are used to represent statistical elements within the signal-to-noise (S/N) ratio calculation method commonly applied in Taguchi analysis:

$\bar{y}$: The mean of the observed values or output response.

$\frac{\bar{y}}{s_{\bar{y}}^2}$: The variance of the observed values.

$log\left(\frac{\bar{y}}{s_{\bar{y}}^2}\right)$: This formula expresses the signal-to-noise ratio for the 'Nominal is the Best' characteristic, indicating how close the process output is to the nominal value while minimizing variability [39, 40].

Response Surface Methodology (RSM) is one of the most prominent statistical methods. First developed by Box and Wilson in 1951, RSM facilitates rapid and sequential improvements in complex industrial processes through optimization and modeling [41]. RSM examines the interactions between different variables and one or more response variables using a series of experiments designed to achieve optimal results. In other words, RSM uses mathematical and statistical methods to define polynomial equations and data sets. In RSM-based optimization processes, when variable levels increase to three, the experimental designs take on a quadratic structure. These models, which include quadratic relationships and interaction terms, are referred to as "second-order models" and are presented in Equation (3): approximately

$$y=\beta_0+\sum_{j=1}^{k}\beta_j x_j+ + \sum_{j=1}^{k}\beta_{jj}x^2{}_j+\sum_{i}^{k-1}\sum_{j}^{k}\beta_{ij}x_i x_j+\varepsilon \quad (3)$$

In Equation 3, a second-order regression model is presented, which is commonly used in the scope of RSM. This model enables the estimation of the effects of linear, quadratic, and interaction terms among the input variables. The equation is particularly effective in multi-factorial experimental designs and optimization studies. Here, y denotes the response variable, β_0 is the intercept, β_j indicates the linear effect of each factor x_j, β_{jj} represents the quadratic effect of x_j, β_{ij} stands for the interaction effect between variables x_i and x_j, ε is the residual (error term), and k is the total number of independent variables in the model [42, 43].

The literature indicates that the optimal stall angle for an aircraft is approximately 5 degrees [44, 45]. Based on this, nine different designs were developed while adhering to this value. The wing design process was conducted using ANSYS-CFD software, and the k-epsilon turbulence model was applied during the analysis. During the solution, a turbulent dissipation rate of 16,238.3 m^2/s^3 and a turbulent kinetic energy of 5.13375 m^2/s^2 were defined. These analyses calculated the Fx and Fz forces required for the geometry. The resulting data were transferred to Minitab 16 software for statistical evaluation of the nine different design criteria. This analysis clarified the impact ratios of all parameters and their effects on the results.

3.2 Specially Developed Wireless Speed Test Prototype

After the ideal geometry was produced, flight tests were started to measure the maximum speed and thrust levels. A special test device was developed for these tests. Arduino Nano, NRF24L01 and GPS Neo 6M modules were used in the creation of the wireless speed measurement system. The system consists of two main components:

Transmitter Unit: Collects speed data and transmits it wirelessly. The GPS Neo 6M module collects speed data and sends it to the Arduino Nano via the serial communication protocol. The Arduino Nano processes this data and transmits it to the receiver unit via the NRF24L01 module. Receiver Unit: Receives the transmitted data and visualizes it on an OLED screen. This unit also contains an Arduino Nano that processes the data from the NRF24L01 module and displays it on the OLED screen. Both units are configured using specific addresses and channels to ensure secure and stable data transmission. As a result, this portable wireless speed measurement device successfully provides real-time speed information to users [46, 47]. The system diagram is shown in Figure 5 and Figure 6.

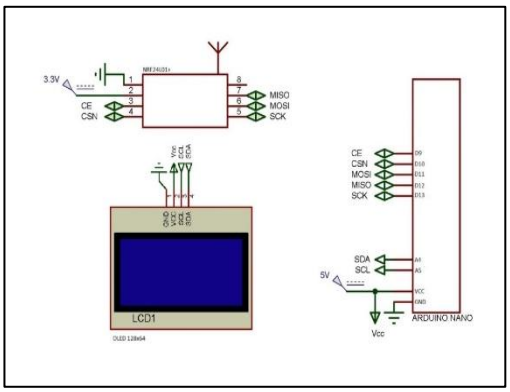

Figure 5. Receiver Circuit Diagram.

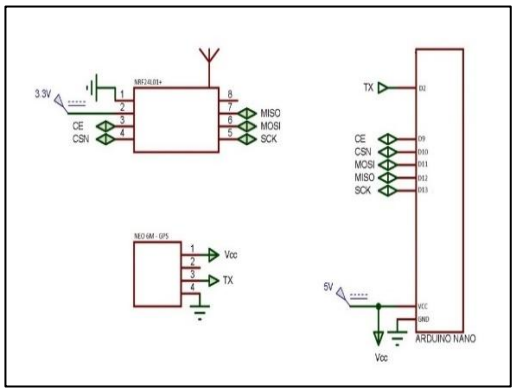

Figure 6. Transmitter Circuit Diagram.

4. RESULTS AND DISCUSSION.

Using Ansys Fluent, the pressure distribution and airflow over the wing were modeled (Figure 7). The results of flow analyses for nine different designs are summarized in Table 2. The highest lift force (Fz) of 253 Newtons was observed in Test 5, while the lowest drag force of 10.2 Newtons was recorded in Test 1. Additionally, the maximum C_L was calculated as 0.66 in Test3, and the highest C_L/C_D ratio was determined to be 17.6 in Test 5. A Parameter: Refers to the side wing angle, which significantly affects C_L and C_X values. Graphical analysis showed that the lift effect was higher at levels 1 and 2. Additionally, C_L/C_D ratio improvements were observed. The maximum Fz effect was observed at level 2, leading to the selection of a 8° angle, ensuring both optimal C_L/C_D and high load-carrying capability at maximum speed.

The abbreviations in Table 2 are as follows; F_X is the force component acting on the horizontal axis and is generally considered as the resistance or thrust force against the forward movement of the aircraft. Fz is the force component acting on the vertical axis and is defined as lift and is the main aerodynamic force that keeps the aircraft in the air. Area expresses the area of the analyzed wing surface in square meters (m^2). C_L is the lift coefficient and is a dimensionless value that defines the magnitude of the lift force produced by the wing. C_D is the drag coefficient and describes the magnitude of the resistance force exerted on the wing due to the airflow. The C_L/C_D ratio is an aerodynamic efficiency indicator showing the relationship between lift and drag. The higher this ratio is, the better the performance of the aircraft.

Table 2. FEM Analysis Results.

Experiment No.	F_X	F_Z	Area	C_L	C_D	C_L/C_D
1	10.24	168.75	0.331	0.6105	0.0369	16.5
2	12.62	215.213	0.399	0.6459	0.0377	17.1
3	19.04	260.84	0.467	0.6688	0.0486	13.8
4	13.45	215.77	0.411	0.6287	0.0390	16.1
5	14.48	253.14	0.484	0.6263	0.0357	17.6
6	13.66	217.37	0.416	0.6257	0.0392	16.0
7	14.86	251.05	0.5	0.6013	0.0354	17.0
8	12.68	203.55	0.4235	0.5756	0.0357	16.1
9	12.68	203.55	0.4235	0.5756	0.0357	16.1

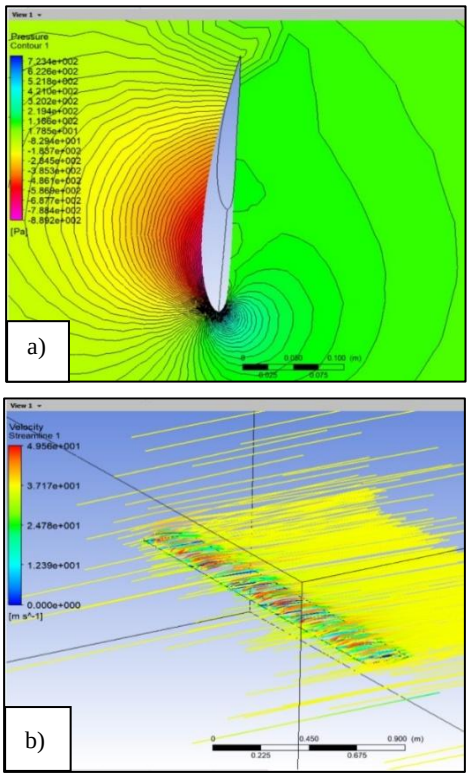

Figure 7. Flow analysis pressure change (a) and air flow pattern (b).

B Parameter: Represents the width of the central wing, which is flat and connects to the fuselage. S/N ratios indicated that selecting level 2 reduces drag force while achieving an ideal C_L/C_D ratio. C Parameter: Refers to the side wing length. While level 3 increases C_L and FZ, level 2 provides lower C_X and C_L/C_D ratios. Although longer side wings enhance payload capacity, they reduce speed. Therefore, an average value of 700 mm was chosen for an optimal design. As a result, a 8° angle, 400 mm central wing length, and 700 mm side wing length were selected as the ideal parameters. Analysis with Taguchi Predict yielded a 98% reliability rate. A drag force of 16.8 N and a lift force of 208.3 N were calculated for this design. Additionally, the design achieved a C_L value of 0.64, forming an ideal flight geometry for the wing.

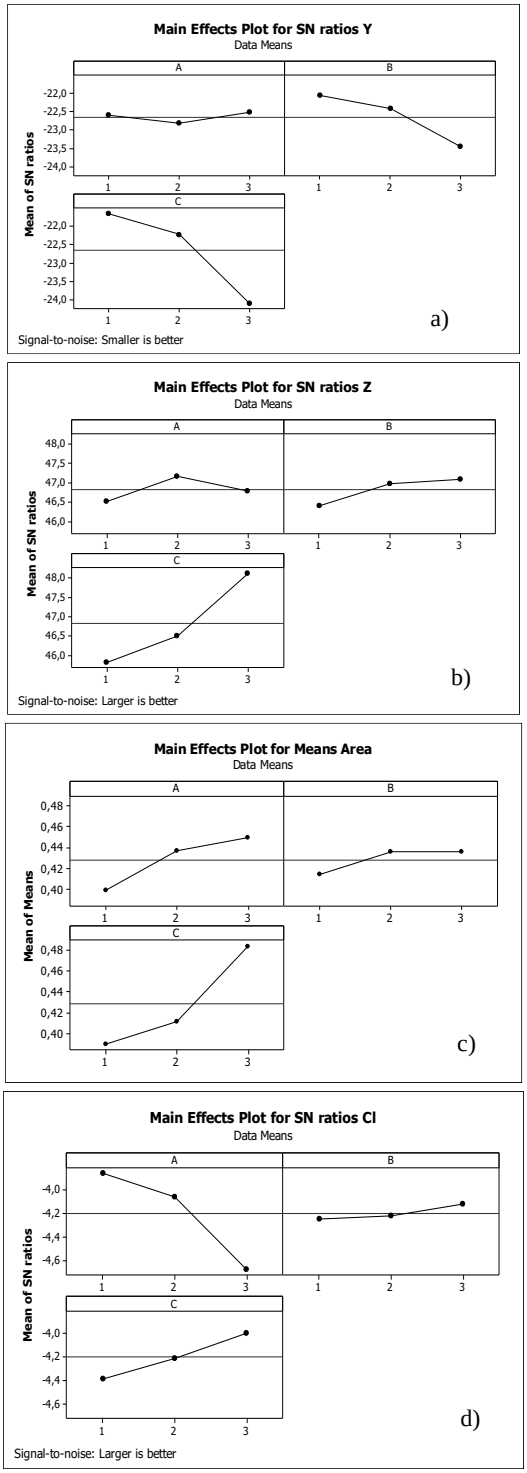

Figure 8. Taguchi method S/N ratios. a) Main Effects Plot for SN ratios Y. b) Main Effects Plot for SN ratios Z. c) Main Effects Plot for Means Area. d) Main Effects Plot for SN ratios C_L

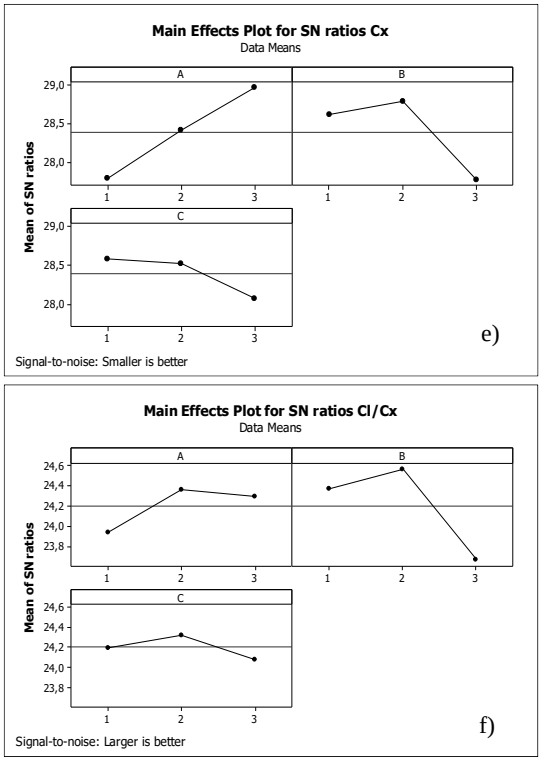

Figure 8. (Cont). Taguchi method S/N ratios. e) Main Effects Plot for SN ratios C_D. f) Main Effects Plot for SN ratios C_L/C_D.

Table 3. Taguchi Predict and Fluent Results.

S/N Ratio	Mean	Analysis	Acurracy
46.3433	208.361	215.2	96.8
-3.89633	0.639	0.645	99.1
24.4273	16.88	17.1	98.7

RSM analysis was conducted in Minitab software, and the accuracy of the results was verified using Probability Plot graphs (Figure 9). All results remained within the desired confidence interval, allowing for the determination of ideal design characteristics. Figure 10 displays Surface Plot graphs, showing result variations based on parameter levels.

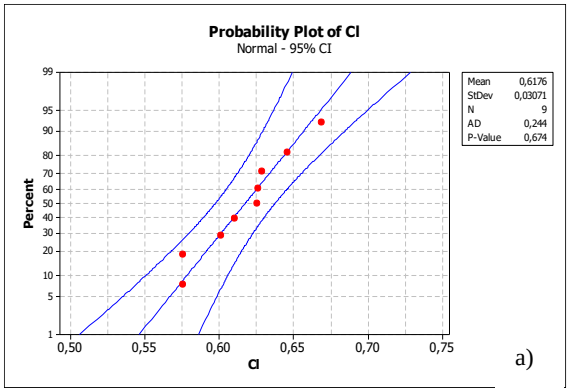

Figure 9. Probability Plot Results. a) Normal Probability Plot for CL Data (95% Confidence Interval).

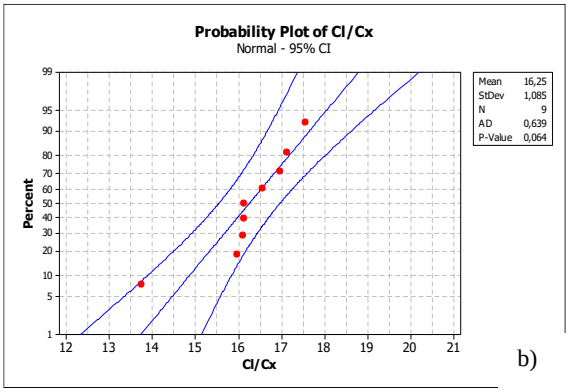

Figure 9. (Cont). Probability Plot Results. b) Normal Probability Plot for C_L/C_D Data (95% Confidence Interval).

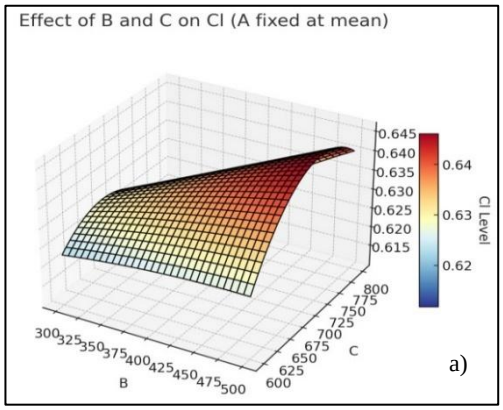

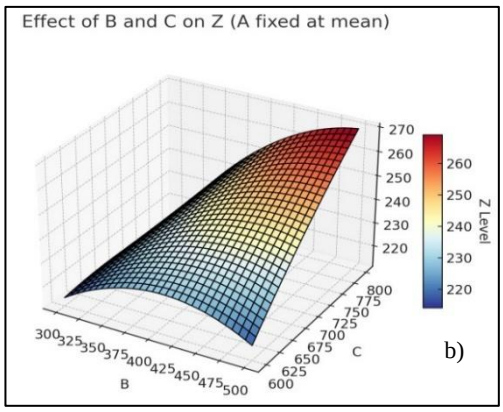

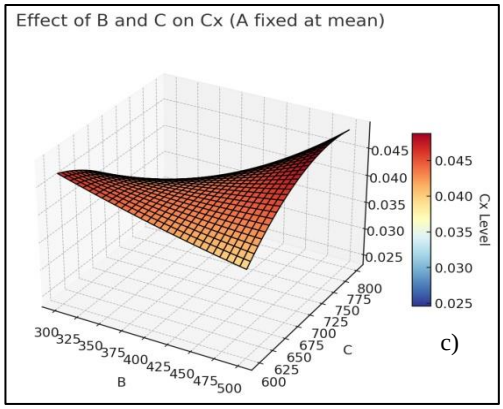

Figure 10. Surface Plot Results. a) Effect of B and C on C_L (A Fixed at Mean). b) Effect of B and C on Z (A Fixed at Mean). c) Effect of B and C on C_D (A Fixed at Mean).

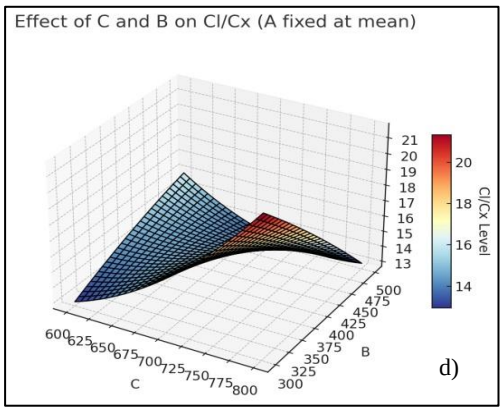

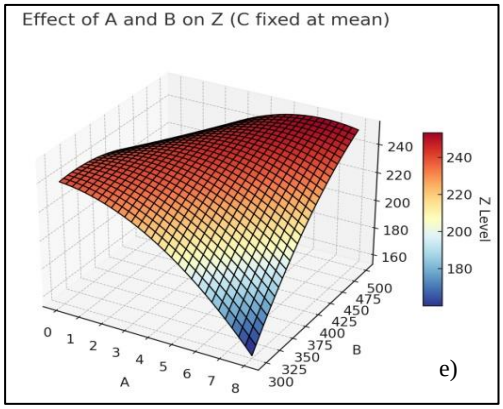

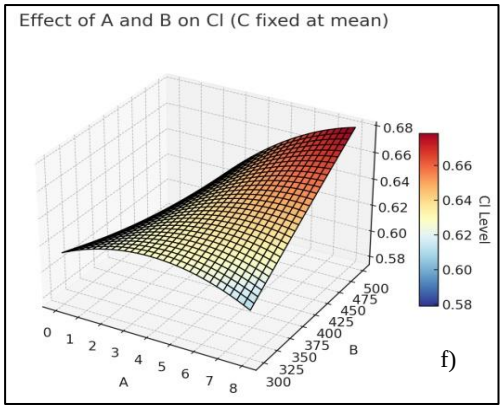

Figure 10. (Cont). Surface Plot Results. d) Effect of B and C on Z (C Fixed at Mean). e) Effect of A and B on C_L (C Fixed at Mean). f) Effect of A and B on Z (C Fixed at Mean).

In this study, the relationships between inputs (A, B, C) and outputs (X, Z, Area, C_L, C_D, C_L/C_D) were examined using RSM. The results obtained from the provided dataset were used to understand the effects of inputs on outputs, identify critical points, and guide process optimization. The roles of A, B, and C at different levels were detailed, and maximum and minimum levels were clearly defined. The input parameter A demonstrated a significant influence, particularly on the outputs C_L and Z. According to the dataset, when A was at lower levels (A=0), both C_L and Z values reached their minimum. Conversely, when A was increased to higher levels (A=8), significant rises in these outputs were observed. For instance, at A=8, B=400, and C=700, the C_L value reached 0.6459, nearing its maximum, while the Z value

peaked at 215.213. These results indicate that A serves as a dominant control factor for these two outputs.

The input parameter B showed a particularly strong effect on Z and a moderate influence on C_L/C_D. An increase in B led to a sharp and high-angled increase in Z, while its effect on C_L/C_D remained more moderate. For example, at B=300, the Z value was recorded at 168.75, whereas increasing B to 500 caused Z to rise sharply to 260.84. In contrast, the C_L/C_X ratio exhibited a steadier rise across the same range of B. These findings highlight the need for careful control of B in process designs where Z output optimization is a priority. The input parameter C was particularly dominant in affecting C_L and C_L/C_D ratios. The data revealed that at the minimum levels of C (C=600), the C_L/C_D ratio remained at a lower value of 16.5. However, when C was increased to its maximum level (C=800), the C_L/C_D ratio rose significantly to 17.6. Similarly, the impact of C on C_L was observed; for instance, at C=600, the C_L value was measured at 0.6105, while at C=800, it increased to 0.6688. These results confirm that C is a critical input parameter for influencing these outputs.

The graphical analysis examining the effects of A, B, and C on key outputs revealed important insights. When A and B were increased together, Z values rose sharply, as shown by a steep gradient on the surface plot. The highest Z value, 260.84, was observed at A = 8 and B = 500, while the lowest value, 168.75, occurred at A = 0 and B = 300. These findings emphasize the need to manage A and B simultaneously to achieve optimal Z performance. Meanwhile, the C_L/C_D ratio was found to be primarily driven by changes in parameter C. For instance, with B fixed at 400, increasing C from 600 to 800 raised the C_L/C_D ratio from 16.1 to 17.6. In contrast, B had a more stable and linear influence. Overall, the analysis highlights the critical role of controlling A and B for optimizing Z, and prioritizing C when aiming to improve the C_L/C_D ratio.

The results of the graphical evaluation revealed that input A leads to a linear increase in C_L output, while input C exhibits a more curvilinear surface trend. A = 8 and C = 800, the C_L output reached 0.6688, approaching the maximum value, while at A = 0 and C = 600, the C_L decreased to 0.6105, the minimum value. These findings show that it is critical to keep A and C inputs at high levels simultaneously in order to maximize C_L output. For enterprises, these data provide important clues for optimizing process designs; for example, while it is recommended to keep inputs A and B high in processes aiming to increase Z output, input C needs to be carefully managed to improve C_L and C_L/C_D ratios. Moreover, it is seen that input B can have positive effects on Z output as a strategic control tool.

In conclusion, this study has thoroughly examined the effects of inputs on outputs and identified critical regions. Proper optimization of inputs at the right levels ensures that the desired performance in outputs is achieved. This study provides a scientific foundation to guide decision-makers in engineering processes, helping them make informed decisions and utilize resources more efficiently. The findings have the potential to enhance output control, providing businesses with a competitive advantage in their operations.

The results were evaluated using the Response Optimizer, and the effects of design parameters were determined. Accordingly, C_L was maximized as the primary objective, while C_D was minimized as the secondary objective. Based on these analyses, the optimal solution was achieved with an 8° side wing angle, 400 mm central wing length, and 700 mm side wing length. These findings were consistent with Taguchi analysis Thus, the ideal wing geometry for UAV operating at low altitudes and 100-meter distances was identified. The RSM Optimizer interface and results are shown in Figure 11. The effects of parameter levels on aerodynamic properties were analyzed using ANOVA (Table 4). The results showed that C_L was most influenced by parameter A (the leading-edge wing) with a 79.8% contribution. C_X was affected by both A and B (central wing length) with a combined influence of 43%. For the C_L/C_D ratio, B (central wing length) had the highest effect with a 79.8% contribution. The side wing length (C parameter) was found to be the least influential, while the side wing angle (A parameter) was the most critical.

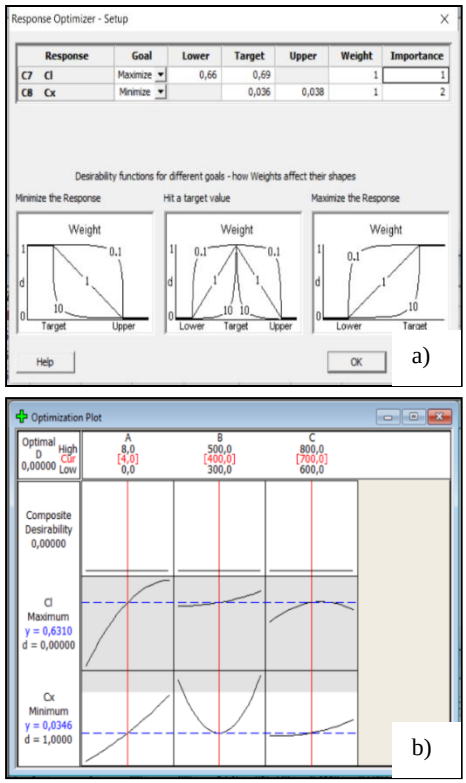

Figure 11. RSM Optimizer definition and results screen. a) Response Optimizer Setup Panel. b) Optimization Plot.

The abbreviations in Table 4 are as follows: Source denotes the factors under study (for example, parameters A, B, and C). D_F (Degrees of Freedom) is the number of independent comparisons used to assess each factor's

contribution to variance. Seq SS (Sequential Sum of Squares) indicates the total variance added to the model by each factor in the order entered. Adj SS (Adjusted Sum of Squares) shows the variance contribution of each factor after accounting for all other factors. Adj MS (Adjusted Mean Square) is the Adjusted SS divided by its DF and is used to gauge the magnitude of each factor's effect. F is the F-statistic, which tests whether a given factor has a statistically significant effect on the dependent variable. P is the p-value indicating the significance level; a value below 0.05 typically signals a significant effect. Finally, % Effect expresses each factor's relative contribution to the total variance as a percentage, highlighting which parameters are most dominant.

Table 4. ANOVA Analysis Results.

	Source	DF	Seq SS	Adj SS	Adj MS	F	P	% Effect
C_L	A	2	0.00537	0.00537	0.002685	6.58	0.132	79.8
	B	2	0.00016	0.00016	7.98E-05	0.2	0.837	2.4
	C	2	0.0012	0.0012	0.000599	1.47	0.405	17.8
	Error	2	0.00082	0.00082	0.000408			
	Total	8	0.00754					
C_D	A	2	4.5E-05	4.5E-05	2.25E-05	1.11	0.474	46.1
	B	2	4E-05	4E-05	1.99E-05	0.98	0.504	40.7
	C	2	1.3E-05	1.3E-05	6.5E-06	0.32	0.757	13.3
	Error	2	4.1E-05	4.1E-05	2.03E-05			
	Total	8	0.00014	0.00014	0.458	0.24	0.808	16.7
C_L/C_D	A	2	0.916	0.916	2.222	1.15	0.464	79.9
	B	2	4.445	4.445	0.1	0.05	0.951	3.5
	C	2	0.2	0.2	1.925			
	Error	2	3.849	3.849				
	Total	8	9.41					

In this study, maximum speed measurements were also conducted for UAVs under different voltage capacities and throttle ranges (40%–100%). The tests included: 5S battery (18.5V) carrying a 4 kg load, 6S battery (22.2V) carrying a 5.2 kg load. The speeds generated by the motors were measured at 40%, 60%, 80%, and 100% throttle settings. During maximum speed tests, the weight was maintained between 2.7–3.2 kg, and the UAV achieved takeoff after a 30-meter run, as reduced weight was critical for speed optimization. Conversely, when testing maximum payload capacity (7–8 kg), the UAV required a takeoff distance of 70–75 meters. The results showed that the 6S battery, despite having only 3.7V higher voltage capacity, provided a significant speed advantage over the 5S battery at all throttle levels. For example, at full throttle, the 6S battery demonstrated a 12.96% higher speed. At 40% throttle, the 5S battery achieved 92 km/h, while the 6S battery reached 101 km/h. This difference increased to 162 km/h versus 183 km/h at full throttle. The table 5 below shows the speed values achieved by 5S and 6S batteries at different throttle levels, along with the percentage increase in speed.

Accordingly, the speed values obtained with 5S and 6S batteries at different throttle levels are presented comparatively in Table 5. As shown in the table, the 6S battery achieved significantly higher speeds than the 5S battery at all throttle levels, reaching a 12.96% increase at full throttle.

Table 5. Comparison of 5S and 6S Battery Speeds.

Throttle Level (%)	5S Battery Speed (km/h)	6S Battery Speed (km/h)	Speed Increase (%)
40%	92	101	9.78%
100%	162	183	12.96%

In the literature, low-altitude optimized UAV are reported to carry a total load of 7–8 kg and achieve average speeds of 115 km/h [4, 48]. This study provides further insights by evaluating the effects of different throttle levels and battery combinations on UAV performance (Figure 12). The discussion emphasized that takeoff distance increases proportionally with payload, affecting the maximum load capacity. For a payload of 7–8 kg, the UAV achieved takeoff within a 70–75meter distance. However, it is projected that increasing the takeoff distance to 100 meters or more would enable the UAV to carry payloads of 10 kg or higher. These findings reveal that payload weight impacts not only speed but also takeoff distance and energy consumption. The test results offer valuable insights into optimizing UAV for varying payloads and takeoff conditions.

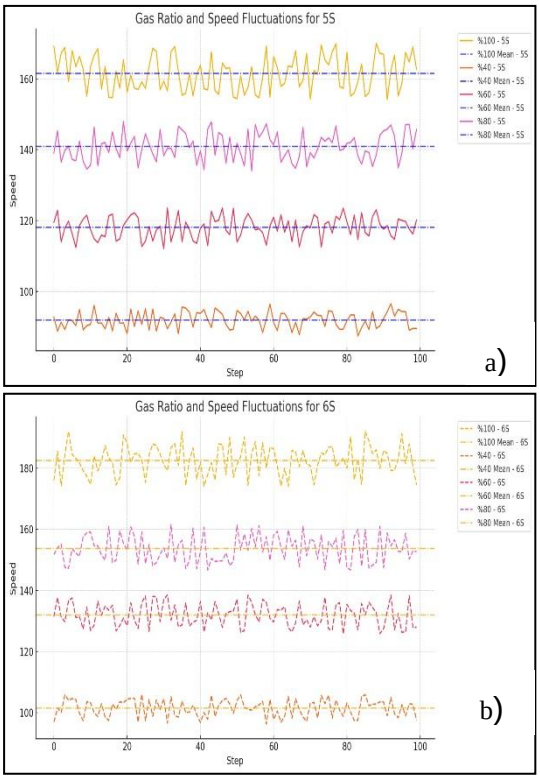

Figure 12. Speed Test, a) 5S Battery Speed Test Results b) 6S Battery Speed Test Results.

5. CONCLUSION.

This study has systematically explored the influence of wing design parameters on key aerodynamic outputs such as C_L, C_D, and their ratio C_L/C_D in low-altitude UAV. Utilizing a hybrid optimization approach that combines RSM, Taguchi analysis, and ANOVA, the

optimal wing configuration was determined to be an 8° side wing angle, 400 mm central wing length, and 700–800 mm side wing length.

The results demonstrated that the side wing angle (A) had the most significant effect on lift performance, while the central wing length (B) predominantly affected aerodynamic efficiency. The side wing length (C), though less influential on its own, became critical when targeting a balanced improvement in both lift and efficiency metrics.

This study not only presents a validated design strategy for UAV wing optimization but also offers a practical reference model for aerospace engineers and UAV developers. The findings emphasize the importance of multi-parameter control in aerodynamic design and contribute to the advancement of efficient, stable, and high-performing UAV in civil and commercial aviation sectors.

These results are consistent with previous studies in the literature. For instance,[49, 50] demonstrated that optimizing the wing structure of fixed-wing UAV can significantly enhance aerodynamic performance. Similarly, [51] utilized genetic algorithms and CFD simulations to improve the C_L/C_D ratio of UAV wings. Our study builds upon these findings by integrating RSM with experimental data, offering a more refined approach to wing geometry optimization.

As a result of this research, an optimized electrically powered UAV capable of operating below cloud cover has been developed, and the following conclusions have been reached:

- The C_L/C_D ratio reached a maximum value of 17.6, demonstrating the aerodynamic efficiency of the design. ANOVA analysis revealed that parameter A (e.g., wing angle), with a 79.8% influence on C_L, is the most critical factor. Additionally, parameters A and B, which have a 43% impact on the C_X ratio, are crucial for controlling speed and energy consumption.
- It was determined that as the lateral wing length increases, the lift force rises, but this results in a slight reduction in speed. The structure designed with a lateral wing length of 700 mm and an 8-degree wing angle provides an ideal solution for low-altitude and short-range missions with a 95% accuracy rate.
- The 6S battery achieved significant speed increases compared to the 5S battery at all throttle levels. For instance, at 40% throttle, the 6S battery achieved a speed of 101 km/h, whereas the 5S battery only reached 92 km/h. At full throttle, the 6S battery demonstrated a speed of 183 km/h, 12.96% higher than the 5S battery.
- Tests conducted with a 7-8 kg payload showed that the UAV required 70-75 meters for takeoff. It is predicted that increasing the payload capacity to 10 kg would require at least 100 meters of takeoff distance.
- At 40% throttle, the 6S battery achieved 101 km/h, while the 5S battery achieved 92 km/h, with this difference measured as 9.8%. At full throttle, the 6S battery reached a speed of 183 km/h, while the 5S battery recorded 162 km/h.
- Tests conducted with lighter payloads (2.7-3.2 kg) observed that the UAV achieved a maximum speed of 183 km/h with only a 30-meter takeoff distance. Reduced weight not only optimized speed but also reduced takeoff distance, enhancing operational flexibility.
- In heavy payload scenarios (7-8 kg), a 70-75 meter takeoff distance led to increased energy consumption. Carrying lighter payloads improved energy efficiency, while the 6S battery's 12.96% speed advantage at full throttle also played a significant role in operational energy savings.
- The lift force of 253 N achieved in the second design was made possible by correctly optimizing the lateral wing length and angle. The lowest drag force, at 10.2 N, was obtained in the first design. Based on the Taguchi analysis, an optimal balance between speed and payload capacity was established with a lift force of 208.3 N and a drag force of 16.8 N.

ACKNOWLEDGE

We sincerely thank Bilecik Şeyh Edebali University Scientific Research Projects Unit for their valuable support within the scope of the project numbered '2022-01.BŞEÜ.03-09'. We would also like to express our gratitude to Düzce Glass Company for their significant contribution to the aircraft construction process.

DECLARATION OF ETHICAL STANDARDS

This article do not require ethical committee permission and/or legal-special permission.

AUTHORS' CONTRIBUTIONS

Osman Özdamar: Design (CAD), production processes (CAM and composites), assembly, execution of flight tests, literature review, data collection, and manuscript writing.

Burak Öztürk: Application of statistical analyses (ANOVA, RSM, Taguchi), evaluation of results, execution of CFD and FEM simulations, aerodynamic modeling and design (CAD), and flight testing.

Emre Can: Literature review, data collection, and manuscript writing.

Cengizhan Abay: Development of the electronic speed measurement hardware and execution of flight tests.

Tufan İnaç: Installation and assembly of electrical and electronic systems, and execution of flight tests.

CONFLICT OF INTEREST

There is no conflict of interest in this study.

REFERENCES

[1] R. Shokirov, N. Abdujabarov, T. Jonibek, K. Saytov, and S. Bobomurodov, "Prospects of the development of unmanned aerial vehicles (UAVs)" ***Technical science and innovation,*** 2020(3):4-8, (2020).

[2] M. T. R. Khan, M. Muhammad Saad, Y. Ru, J. Seo, and D. Kim, "Aspects of unmanned aerial vehicles path planning: Overview and applications" ***International Journal of Communication Systems,*** 34(10):e4827. (2021).

[3] A. Martian, C. Paleacu, I.-M. Marcu, and C. Vladeanu, "Direction-finding for unmanned aerial vehicles using radio frequency methods" ***Measurement,*** 235:114883. (2024).

[4] S. A. H. Mohsan, M. A. Khan, F. Noor, I. Ullah, and M. H. Alsharif, "Towards the unmanned aerial vehicles (UAVs): A comprehensive review" ***Drones,*** 6(6):147. (2022).

[5] E. E. Elmas and M. Alkan, "Collision Avoidance for Autonomous Unmanned Aerial Vehicles with Dynamic and Stationary Obstacles" ***Politeknik Dergisi,*** pp. 1-1. (2024).

[6] N. Can and M. Kahveci, "İnsansız hava araçları: Tarihçesi, tanımı, dünyada ve Türkiye'deki yasal durumu" ***Selcuk University Journal of Engineering, Science and Technology,*** 5(4):511-535, (2017).

[7] L. Rabiu, A. Ahmad, and A. Gohari, "Advancements of unmanned aerial vehicle technology in the realm of applied sciences and engineering: A review" ***Journal of Advanced Research in Applied Sciences and Engineering Technology,*** 40(2):74-95, (2024).

[8] A. S. Akgül and A. Hacıoğlu, "To design and build of a surveillance/attack mini unmanned aerial vehicle (UAV)" ***Journal of Aeronautics and Space Technologies,*** 4(3):1-6, (2010).

[9] M. Danışmaz, D. Atılğan, and F. Karaca, "Sabit Kanatli Mini İha'lar İçin Kanat Profili Tasarimi Ve Analizi".

[10] S. Gudmundsson, "General aviation aircraft design: Applied Methods and Procedures". ***Butterworth-Heinemann***, (2013).

[11] D. Raymer, "Aircraft design: a conceptual approach". ***American Institute of Aeronautics and Astronautics, Inc.***, (2012).

[12] Y. Wang, K. Zhao, X.-Y. Lu, Y.-B. Song, and G. J. Bennett, "Bio-inspired aerodynamic noise control: a bibliographic review" ***Applied Sciences,*** 9(11):2224. (2019).

[13] Y. Wei, F. Xu, S. Bian, and D. Kong, "Noise reduction of UAV using biomimetic propellers with varied morphologies leading-edge serration" ***Journal of Bionic Engineering,*** 17:767-779. (2020).

[14] T. J. Mueller, "Fixed and flapping wing aerodynamics for micro air vehicle applications". ***AIAA***, (2001).

[15] Y. Celik, "A comparative aerodynamic analysis of NACA and NREL aerofoils for darrieus turbines using CFD" ***International Journal of Innovative Engineering Applications,*** 6(1):111-117. (2022).

[16] Y. F. Görgülü, M. A. Özgür, and R. Köse, "CFD analysis of a NACA 0009 aerofoil at a low reynolds number" ***Politeknik Dergisi,*** 24(3):1237-1242. (2021).

[17] D. A. Gök and K. Alnimer, "Characterization of NACA 2412 and NACA 4412 airfoils: Effects of angle of attack on aerodynamics coefficients" ***Journal of Thermal Engineering,*** 10(6):1524-1538. (2021).

[18] Y. Luo, G. Pan, Q. Huang, Y. Shi, and H. Lai, "Parametric geometric model and shape optimization of airfoils of a biomimetic manta ray underwater vehicle" ***Journal of Shanghai Jiaotong University (Science),*** 24:402-408. (2019).

[19] K. Upasena, U. Weerathunga, J. Abeygoonewardena, and R. Bandara, "Design of a new aircraft wing inspired by the Magnificent Frigate bird". (2019).

[20] D. S. Martin, "An Investigation of Avian Wing Tip Vortex Generation Using a Biomimetic Approach," ***California Polytechnic State University***, (2017).

[21] V. E. Focke, A. B. Kesel, and A. Baars, "Flying fish: Biomimetic potential for wing in ground effect crafts?" ***Bionik: Patente aus der Natur***. (2016).

[22] J. T. Murphy, "Experimental investigation of biomimetic wing configurations for Micro Air Vehicle applications". ***Iowa State University***, (2008).

[23] A. Risanthia, T. Phiboon, S. Bureerat, A. Pichitkul, S. Tantrairatn, and A. Ariyarit, "UAV Wing Design via Efficient Global Optimization" in *2024 16th International Conference on Knowledge and Smart Technology (KST)*, of Conference: ***IEEE***, pp. 62-66. (2024)

[24] S. G. Kontogiannis and J. A. Ekaterinaris, "Design, performance evaluation and optimization of a UAV" ***Aerospace science and technology,*** 29(1):339-350. (2013).

[25] S. Evran and S. Z. Yıldır, "Numerical and statistical aerodynamic performance analysis of NACA0009 and NACA4415 airfoils" ***Politeknik Dergisi,*** 27(3):849-856. (2023).

[26] R. Jain, M. S. Jain, and M. L. Bajpai, "Investigation on 3-d wing of commercial aeroplane with aerofoil naca 2415 using cfd fluent" ***IRJET,*** 3(6):243-249. (2016).

[27] H. Demir and N. Kaya, "Bir Hava Aracının Çok Amaçlı Kanat Kiriş Kesit Optimizasyonu" ***Politeknik Dergisi,*** pp. 1-1.

[28] B. Öztürk and F. Öncü, "Optimization of thrust and fuel efficiency in low-altitude UAV engines through experimental design and statistical analysis" ***Journal of the Brazilian Society of Mechanical Sciences and Engineering,*** 47(3):131. (2025).

[29] J. D. Anderson and M. L. Bowden, "Introduction to flight". ***McGraw-Hill Higher Education New York, NY, USA***, (2005).

[30] D. Küchemann, "The aerodynamic design of aircraft". ***American Institute of Aeronautics and Astronautics, Inc.***, (2012).

[31] A. K. Kundu, "Aircraft design". ***Cambridge University Press***, (2010).

[32] A. J. Keane, A. Sóbester, and J. P. Scanlan, "Small unmanned fixed-wing aircraft design: a practical approach". ***John Wiley & Sons***, (2017).

[33] T. Liu, "Evolutionary understanding of airfoil lift" ***Advances in Aerodynamics,*** 3(1):37. (2021).

[34] C. Lee, S. Kim, and B. Chu, "A survey: Flight mechanism and mechanical structure of the UAV" ***International Journal of Precision Engineering and Manufacturing,*** 22(4):719-743. (2021).

[35] A. Lamsal, A. K. Mishra, S. Prajapati, and J. William, "Theoretical and Computational Study on Swept Back Wing for Variable Mach Ranges" ***International Journal of Enhanced Research in Science, Technology & Engineering,*** 11(10):22-29. (2022).

[36] C. J. Ejeh, G. P. Akhabue, E. A. Boah, and K. K. Tandoh, "Evaluating the influence of unsteady air density to the aerodynamic performance of a fixed wing aircraft at

different angle of attack using computational fluid dynamics" ***Results in Engineering,*** 9:100037. (2019).
[37] R. A. Fisher and R. A. Fisher, "The design of experiments". ***Springer***, (1971).
[38] E. Nas and B. Öztürk, "Optimization of surface roughness via the Taguchi method and investigation of energy consumption when milling spheroidal graphite cast iron materials" ***Materials Testing,*** 60(5):519-525. (2018).
[39] İ. Karadağ, S. Dündar, and Ö. F. Gürcan, "Taguchi Deney Tasarımı ile Fiber Optik Kablo Üretimi Proses Optimizasyonu" ***Fırat Üniversitesi Mühendislik Bilimleri Dergisi,*** 36(2):743-754. (2024).
[40] N. Ghosh, P. K. Pal, and G. Nandi, "GMAW dissimilar welding of AISI 409 ferritic stainless steel to AISI 316L austenitic stainless steel by using AISI 308 filler wire" ***Engineering science and technology, an international journal,*** 20(4):1334-1341. (2017).
[41] O. Özdamar and B. Öztürk, "A New Specific Carbon Footprint (Scf) Theory Of Flow Rate And Energy Consumption Variations Of An Industrial Internal GEAR PUMP" ***International Journal of 3D Printing Technologies and Digital Industry,*** 8(3):428-436. (2024).
[42] V. Gaitonde, S. Karnik, and J. P. Davim, "Minimising burr size in drilling: integrating response surface methodology with particle swarm optimisation" in Mechatronics and Manufacturing Engineering: ***Elsevier***, pp. 259-292 (2012).
[43] F. Sönmez, H. Başak, and Ş. Baday, "Haddeleme işleminin yüzey yanit yöntemi ile analizi" ***Gazi University Journal of Science Part C: Design and Technology,*** 4(4):275-283. (2016).
[44] G. Ramanan, P. R. Krishnan, and H. Ranjan, "An aerodynamic performance study and analysis of SD7037 fixed wing UAV airfoil" ***Materials Today: Proceedings,*** 4:2547-2552. (2021).
[45] M. Altay and E. Türkeş, "Sabit Kanatlı İHA'da Kanat Geometrisinin Aerodinamikteki Etkileri" ***Kirklareli University Journal of Engineering and Science,*** 10(2):363-376. (2024).
[46] M. Mahbub, "Design and implementation of multipurpose radio controller unit using nRF24L01 wireless transceiver module and Arduino as MCU" ***International Journal of Digital Information and Wireless Communications,*** 9(2):61-72. (2019).
[47] N. Noviarianto, T. Turahyo, P. T. Kusumartono, and A. Anwar, "Implementation of Low Cost Real Time GPS Using the Haversine Method in Fishermen Electronic Navigation". (2023).
[48] J. E. Smart, "Unmanned Systems and Platform Options for Environmental Studies," ***Pacific Northwest National Lab.(PNNL), Richland, WA (United States)***. (2017).
[49] J. Yu, "Design and optimization of wing structure for a fixed-wing unmanned aerial vehicle (UAV)" ***Modern Mechanical Engineering,*** 8(4):249-263. (2018).
[50] K. R. Sekar, M. Ramesh, R. Naveen, M. Prasath, and D. Vigneshmoorthy, "Aerodynamic design and structural optimization of a wing for an Unmanned Aerial Vehicle (UAV)" in *IOP conference series: materials science and engineering*, of Conference, ***IOP Publishing***, 764(1): 012058, (2020).
[51] M. Rostamzadeh-Renani *et al.*, "A multi-objective and CFD based optimization of roof-flap geometry and position for simultaneous drag and lift reduction" ***Propulsion and Power Research,*** 13(1):26-45. (2024).